Materials Science & Engineering B 226 (2017) 29–38

Contents lists available at ScienceDirect

Materials Science & Engineering B

journal homepage: www.elsevier.com/locate/mseb

3D printing of highly flexible supercapacitor designed for wearable energy storage

Milad Areir*, Yanmeng Xu, David Harrison, John Fyson

Department of Design, College of Engineering and Physical Sciences, Brunel University London, Uxbridge UB8 3PH, UK

ARTICLE INFO

Keywords:
3D printing technology
Electrical double-layer capacitors (EDLCs)
Flexible supercapacitor
Wearable energy storage
Bending test

ABSTRACT

The rapid development of flexible energy storage devices is crucial for various applications. However, it is still difficult to manufacture functional flexible electrochemical double layer capacitors (EDLCs) in one single process due to many different types of materials being used in EDLCs. This paper presents a novel method of manufacturing highly flexible EDLCs by using an open source 3D printer. The EDLC components were fabricated using a single paste extrusion in a layer wise manner. The detailed fabrication process for a highly flexible EDLCs device has been demonstrated, where acetoxy silicone was used as the flexible substrate. The purpose of this study has been to develop a single continuous manufacturing process for EDLC and to investigate the electrochemical performances of 3D printed flexible supercapacitors. Mechanical bending tests were carried out to prove the stability of the electrochemical performance and flexibility of the 3D printed supercapacitors.

1. Introduction

The development of energy storage devices has faced major technological challenges during the past few decades. Electrical double layer capacitors (EDLCs) are a promising competitor for alternative energy storage because of their low-cost, high power density and long cycle life. Being flexible is one of the critical demands for the recent development of energy storage devices [1–3]. Recently, EDLCs and microsupercapacitors have been studied and manufactured by a number of companies around the world with different novel techniques, such as spray coating, 3D double extrusion, microextrusion, etc [4–25]. The above techniques, however, are often costly or not able to process all the materials necessary for making EDLCs. Thus, a combination of several processes has been required to fabricate a complete and workable EDLC. 3D printers developed for additive manufacture have the ability to create almost any geometrically complex shape and pattern in a wide range of materials and offer highly precise conformal depositions [26–28]. The advantages of additive manufacture have been applied previously in the development of flexible supercapacitors, but it is still a challenge to achieve a good and stable working performance, particularly under mechanical bending conditions [29,30]. Other advantages of this process are that it allows complex shaped supercapacitors to be made, flexibility in packaging due to a variety of 3D shapes, and the manufacturing of 3D electronic structures for consumers. Moreover, compared to other 3D printing methods, 3D paste printing allows a wide selection of composite materials to be deposited by quickly changing syringes. 3D paste printing does not need complicated post-processing such as thermal sintering, a mask to transfer pattern or heat to laminate EDLCs. The use of 3D paste printing is easy, and allows more rapid prototyping of EDLCs for research purposes and achieves end properties of 3D EDLCs.

This study has addressed the above key challenges and developed a novel 3D printing method for manufacturing flexible supercapacitors, by one single continuous process and using low-cost flexible silicone structural materials that are compatible with the electrode, current collector and electrolyte materials.

2. Materials used for EDLCs

2.1. Materials

Dow Corning® acetoxy silicone supplied by Screwfix® was used for substrate and package material. The mixture of silver powder (Ag) purchased from Gwent Group® and zinc metal powder (Zn, MW 65.38) was used for current collector paste. All other materials including the activated carbon particle powder (AC, AR grade, Cat. No. 05105, MW 12.01 g mol^{-1}), sodium carboxymethyl cellulose (CMC, MW 250,000), polyvinylidene fluoride-co-hexafluoropropylene (PVDF-HFP, MW 400,000–130,000), polyvinyl alcohol (PVA, MW 146,000–186,000, 99+% hydrolysed), 1-methyl-2-pyrrolidinone (NMP, 1.028 g ml^{-1}) and phosphoric acid (H_3PO_4, 6 M) were supplied by Sigma-Aldrich®.

* Corresponding author.
E-mail address: milad.areir@brunel.ac.uk (M. Areir).

http://dx.doi.org/10.1016/j.mseb.2017.09.004
Received 7 June 2017; Received in revised form 14 August 2017; Accepted 4 September 2017
Available online 11 September 2017

2.2. Preparation of the activated carbon slurry

In order to reduce the size of the activated carbon (AC) particles and to ensure a uniform deposition of AC slurry through a tiny 0.6 mm tapered nozzle, a ball-milling process was used. 100 g of AC powder was added into 50 mL of carbon-based Chinese ink, and 100 mL of distilled water, and milled for 72 h. The average particle diameter is 0.4 μm. Then 5 g of the milled AC powder was heated at 150 °C in an oven to allow the solvent, mostly water, to evaporate. 2.6 g PVA powder was dissolved in 20 ml distilled water at 50 °C for 1 h under magnetic stirring. The dry AC power was mixed with the PVA gel solution under stirring at room temperature for 24 h. To ensure the homogeneity of the AC slurry 8 mL H_3PO_4 and 1 g of 5% CMC was added.

2.3. Preparation of the gel electrolyte

The PVA gel electrolyte used in this study was an important component for flexible EDLCs and its properties significantly affected the EDLC's electrochemical performance. To prepare an aqueous solution of PVA, 2.5 g PVA powder was mixed with 30 mL distilled water and was stirred at 50 °C for 1 h until fully dissolved. To avoid a rough layer and to get more sticky 1.5 g CMC of 5% was then mixed with the PVA solution followed by 18 mL 6 M H_3PO_4 with magnetic stirring overnight until completely homogeneous.

2.4. Preparation of the current collector paste

It was critical to prepare a conductive paste with a good bonding to the substrate in 3D printing, especially as silicone was used as the substrate material. 1 g PVDF-HFP pellets were dissolved in 15 mL NMP at 40 °C for 1 h first. After that, 4.5 g zinc metal powder was mixed with 5 g silver powder (Ag) and added to the solvent/polymer mixture and kept stirring overnight. PVDF as a type of piezoelectric polymer enhanced the bonding of silver and zinc particles therefore improving the conductivity of the current collector.

3. Manufacturing process and measurement for EDLCs

3.1. Design of the structure of printable wearable EDLC

Fig. 1 shows the schematic diagram of an EDLC designed for this study. Due to the working mechanisms, there are four layers of materials on each side of an EDLC, i.e. silicon substrate, current collector, AC material, and gel electrolyte. This EDLC was also designed as a wearable device, i.e. a bracelet, thus the structure of the supercapacitor designed for this study included a locking mechanism to allow the complete product to be worn around the wrist as a bracelet.

3.2. Manufacturing process

Paste deposition by 3D printing is a promising manufacturing method for controlling the deposition layers, and it can provide accurate and complex structured devices. In this study, a paste extruder (Discov3ry®) was employed to print all the different types of materials for the EDLC. As shown in Fig. 2(a) the paste extruder was attached to, and controlled by, a commercial 3D printer (Ultimaker®). Fig. 2 shows the manufacture processes of a flexible EDLC, and Table 1 lists the manufacturing process parameters. The EDLCs components were deposited in a 100% fill density in grid patterns to make the device robust. Fig. 2(b) depicts the frame part of an EDLC printed by depositing acetoxy silicone material on a build platform covered with Teflon paper, which was used for easy removal when the wet silicone is dried. Subsequently, the frame part printed was left to cure for 2 h. In addition, 5% CMC binder was coated by spreading method on surface of the silicone substrate in order to help the current collector layer stick onto the silicone substrate better. Fig. 2(c) shows the current collector material to be deposited on silicone layer and kept for 2 h to fully cure and adhere to the silicone substrate. Next, the AC electrode layer of 0.6 mm thickness was deposited with a dimension of 163 mm × 5 mm as shown in Fig. 2(d). Following this, the gel electrolyte of PVA/H_3PO_4 was deposited onto the electrodes and they were kept in a vacuum desiccator for an hour to allow the infiltration of the PVA/H_3PO_4 electrolyte into the carbon particle pores fully, as illustrated in Fig. 2(e). The components already built and fully dried were then returned to the platform of the 3D printer to deposit another layer of silicone around the edge to act as a gasket. The other side of the EDLC was printed the same as described above. Finally, the two sides were sealed together as a complete EDLC, as revealed in Fig. 2(f).

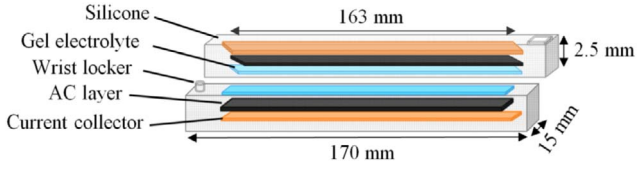

Fig. 1. Schematic of the structure of printable wearable EDLC.

In total four EDLCs (designated as *C1*, *C2*, *C3* and *C4*) have been manufactured under the same conditions in this study to investigate the reproducibility of the manufacturing process and the stability of the electrochemical performance of the EDLCs.

3.3. Measurement of the electrochemical properties

An electrochemical workstation (VersaSTAT 3.0) was set up to measure the electrochemical performance of the EDLCs printed. The electrochemical performance was evaluated by cyclic voltammetry (CV) and galvanostatic charge/discharge (GCD) tests. Electrochemical impedance spectra (EIS) were measured at an open circuit potential of 0 V between the frequencies from 0.01 Hz to 100 kHz with 10 points per decade. The capacitance (C) can be calculated from the CV curve measured using:

$$C = \frac{Q_{total}/2}{\Delta V} \tag{1}$$

Where, C is the capacitance in farads (F), Q_{total} is the supercapacitor charge in coulombs (C), and ΔV is the voltage range in volts (V).

The area specific capacitance (C_a) of the supercapacitor can be calculated from the CV curves using:

$$C_a = (1/2A(\Delta V/\Delta t)(V_f - V_i)) \int_{V_i}^{V_f} I(V)\Delta V \tag{2}$$

Where, A is the area of the electrodes (cm^2), ΔV/Δt is the voltage scan rate ($V\ s^{-1}$), V_f and V_i are the potential limits of the CV curve, and $\int_{V_i}^{V_f} I(V)\Delta V$ is the numerically integrated area of the CV curve.

During the GCD test, the capacitance can be calculated at a constant current of 15 mA by:

$$C = \frac{i.\Delta t}{\Delta V} \tag{3}$$

Where, i is the discharge current in amperes (A), Δt is the discharging time (s) and ΔV is the voltage of the discharge (V). In addition, the specific capacitance (C_s) of the supercapacitor can be calculated using:

$$C_s = \frac{2C}{m} \tag{4}$$

Where, C is the capacitance in farad (F) calculated by GCD, m is the total mass of the active material used for one single electrode (g).

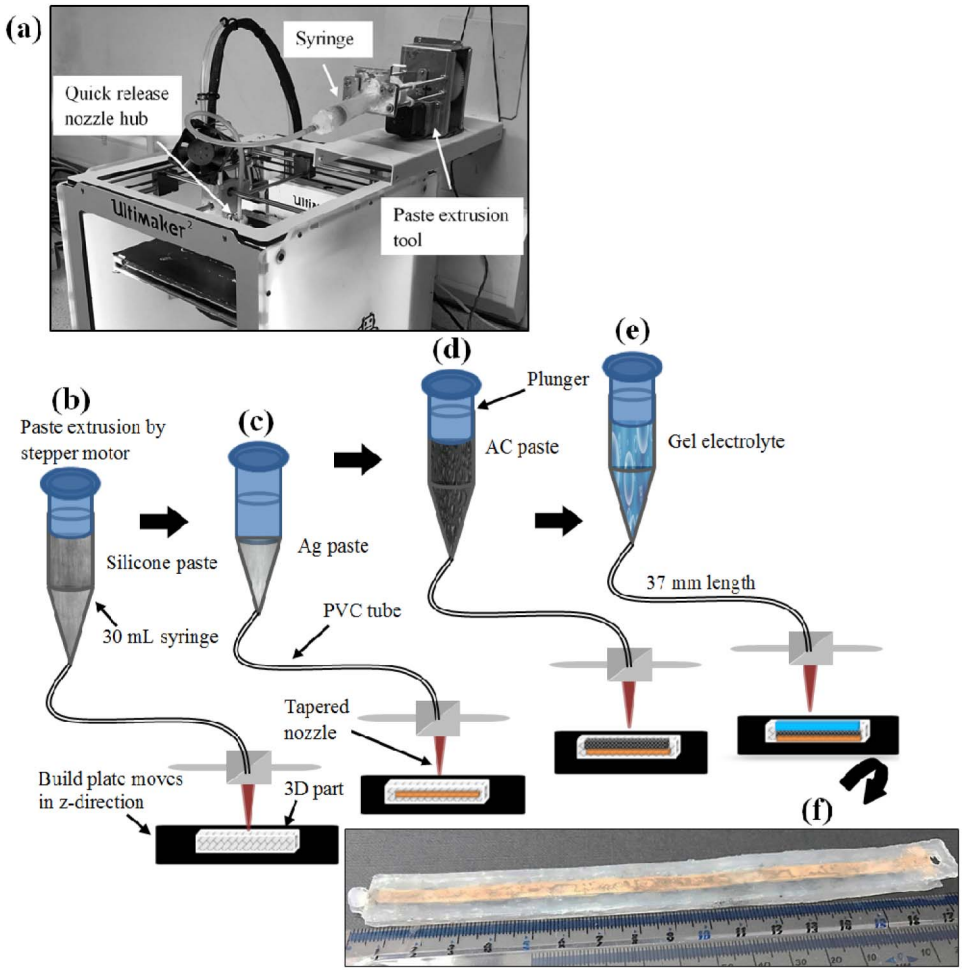

Fig. 2. A schematic representation of the 3D flexible EDLCs manufacture.

Table 1
3D process parameters used for manufacturing the EDLC.

Pastes	Layer height (mm)	Nozzle diameter (mm)	Printing speed (mm s^{-1})	Feed-rate (steps mm^{-1})
Silicone & AC	0.6	0.6	90	18,000
Electrolyte & conductive paste	0.6	0.6	60	15,000

4. Result and discussion

C1 was selected as a sample for assessing the electrochemical performance of a single supercapacitor designed and manufactured in this study. *C1* and *C2* were selected for evaluating the combined electrical circuit.

4.1. Evaluation of the 3D printing process

Fig. 3 shows a half (one side) of the EDLC successfully printed with 2 layers on 2.5 mm thick silicon substrate, each layer of the material printed was about 0.6 mm thick and the total printing time spent was approximately 8 min. The total mass of printed AC electrode was 2 g for both EDLC frames at 100% fill density. Overall, the 3D printed flexible EDLC showed that the adhesion between different material layers was strong and there was no leakage. The grid pattern selected for different layers of materials displayed a solid structure and robust final product. The disadvantage of the paste extruder driven by a stepper motor was that it was difficult to have a consistent deposition rate when the material's viscosity was too high with the tiny 0.6 mm diameter tapered printing nozzle. Therefore, the silicone and AC slurry had to be fresh material, with a low viscosity, in order to obtain a consistent deposition and an accurate dimension for each layer of the material. The PVA/H_3PO_4 gel electrolyte and its viscosity and smooth flow could be manipulated by adding H_3PO_4 acid if necessary.

The scanning electron microscopy (SEM) of the surface morphology of the 3D printed AC slurry electrode as shown in Fig. 4. It was measured on a Zeiss (Model SUPRA 35 VP), and operated at an acceleration voltage of 20 kV. It reveals that the AC slurry consists of PVA binder and has a pores structure that was impregnated with H_3PO_4 electrolyte.

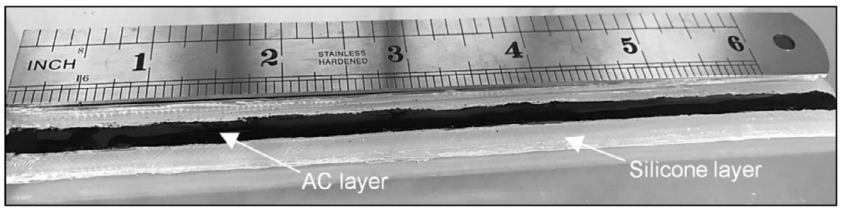

Fig. 3. 3D printed EDLC part of the silicone substrate and AC layers.

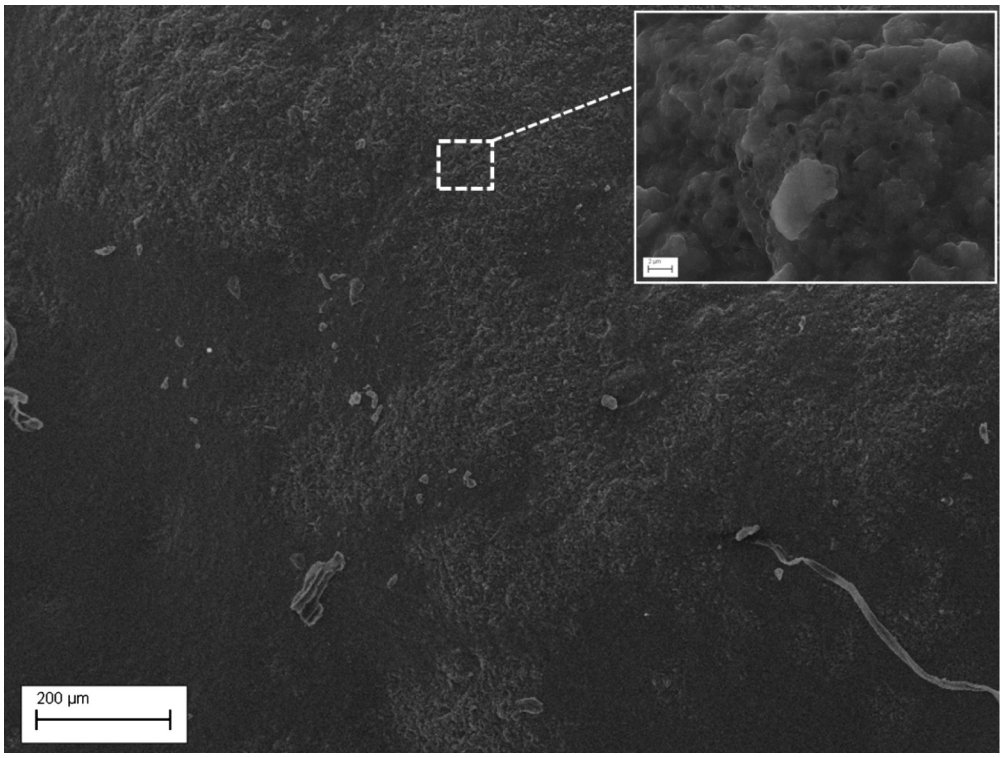

Fig. 4. SEM image of 3D printed AC electrode layers.

The small number of holes is intriguing. It might be due to the trapped air when the paste was extruded or the front filling method of the AC paste has entrapped some air.

4.2. CV characterization

CV tests were performed to determine the capacitance of the printed AC electrodes. All CV curves were recorded with an applied potential from 0 to 0.8 V. Fig. 5 shows the typical charge-discharge profile of the flexible EDLC (*C1*). *C1* delivered a capacitance of 1.4, 0.7, and 0.2 F at the scan rate of 20, 50, and 100 mV s^{-1}, respectively, calculated by Eq. (1). It can be seen that the charging current decreases with the decrease of scan rate, which leads to an increase of the capacitance. The C_a of the flexible EDLC based on both electrolytes calculated from the CV curves by Eq. (2) were 1.48, 0.45, and 0.13 F cm^{-2} at scan rate of 20, 50, and 100 mV s^{-1}, respectively. The specific capacitance of the EDLC depends on the specific surface area of AC electrode in contact with the electrolyte. The Chinese ink used in the AC material may also provide an extra accessible specific surface area in this case. The capacitance increased with the decrease of the scan rate because at the lower scan rate the ions could travel deeper inside the AC material leading to a better surface coverage reaction.

4.3. GCD characterization

Fig. 6(a) shows five cyclic charge-discharge curves measured for *C1* at a constant current of 15 mA. By applying the potential to the electrodes, ions were pulled to the surface of the electrical double layer and

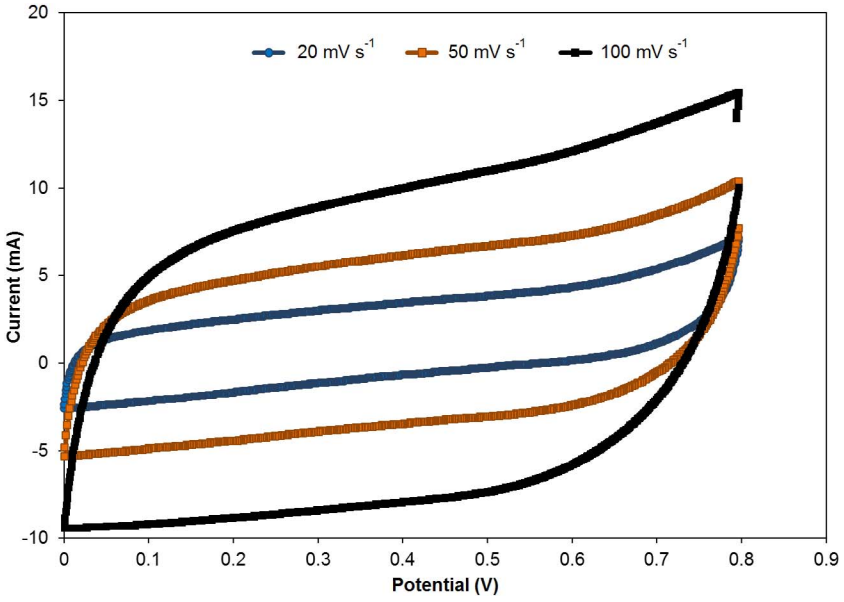

Fig. 5. CV curves of printed flexible EDLC recoded at different scan rates of 20, 50, 100 mV s^{-1}.

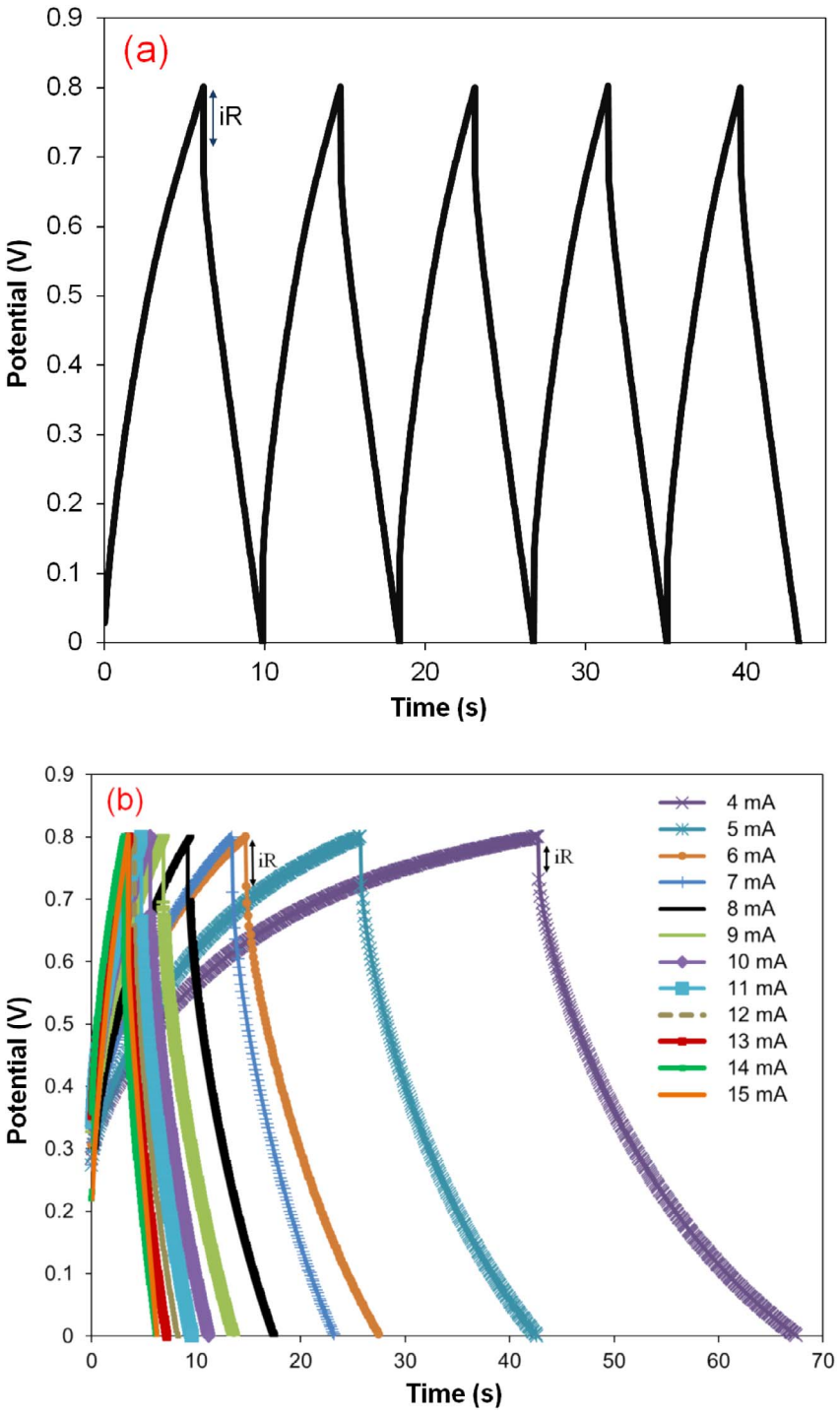

Fig. 6. (a) Constant current GCD curve of flexible electrodes at current of 15 mA; (b) GCD curve recorded at different charge currents.

supercapacitor was charged. Inversely, they moved far away when discharging the supercapacitor and the dielectric material (PVA/H_3PO_4) was responsible for preventing the two AC electrodes from contacting or shorting. The curve is almost linear within the whole potential range, which shows an excellent supercapacitor performance. There was an iR drop because of the equivalent series resistance (ESR) of the EDLC and discharge current, which is the voltage drop (V_{iR}) at the beginning of each discharge curve, as shown in Fig. 6(a). The iR drop for the electrolyte was about 0.12 V. The iR compensation technique (iR_{comp}) using the electrochemical workstation in an auto-ranged experiment showed the resistance to be 5.5 Ω. The minimum iR_{comp} (1.96 Ω), is similar to the ESR and shows a good contact between printed AC and current collector and there was no corrosion on current collector caused by PVA/H_3PO_4. The discharging time of the GCD process was 4 s. The capacitance can be directly calculated by GCD using Eq. (3), which was 0.1 F and almost half of the capacitance value calculated by CV at the scan rate of 100 mV s^{-1}. This is because the high current of 15 mA was applied constantly during the GCD test at 0.8 V, whereas the maximum current observed from the CV test was 15 mA at the scan rate of 100 mV s^{-1} (shown in Fig. 5). It has been proved above that the higher current applied the lower the capacitance that can be obtained. It is considered that the high current of 15 mA and the thickness of 0.6 mm of the AC electrodes lead to a low operation of kinetic movement of ions. In addition, the low iR_{comp} and the maximum current of 15 mA at the scan rate 100 mV s^{-1} may lead to some energy loss. Fig. 6(b) shows that the iR increased when the current increased,

Table 2
3D printing techniques for fabrication of supercapacitors.

Fabrication process	Electrode/Electrolyte	Performance				Ref.
		Specific capacitance	Energy density	Power density	Cycling stability	
3D printing direct-ink writing	Graphene aerogel/KOH	63.6 F g^{-1}	0.14 mWh cm^{-3}	49.4 mW cm^{-3}	95.5% after 10,000 cycles	[32]
3D laser direct writing	rGO/Au/PVA-H_2SO_4	3.8 mF cm^{-2}	n/a	n/a	50% after 10,000 cycles	[33]
3D micro extrusion	rGO/PVA-H_2SO_4	41.8 F cm^{-3}	7.6 mWh cm^{-2}	29.2 mW cm^{-2}	41% after 10,000 cycles	[6]
3D laser direct writing	Polyimide/PVA-H_2SO_4	2.3 mF cm^{-3}	n/a	n/a	96% after 2000 cycles	[34]
3D printing selective laser melting	Ppy/PVA-H_3PO_4	2.4 F cm^{-3}	213.5 Wh m^{-3}	15.0 kW m^{-3}	78% after 1000 cycles	[35]
3D printing (FDM)	Graphene PLA/PVA-H_2SO_4	485.4 μF g^{-1}	n/a	n/a	33% after 200 cycles	[36]
Micromachining technique (LIGA-like)	Ppy/$LiClO_4$-H_2O-PVA	0.03 F cm^{-2}	n/a	2.2 mW cm^{-2}	n/a	[37]
3D paste process	AC/PVA-H_3PO_4	1.48 F cm^{-2}	0.064 Wh kg^{-1}	57.6 W kg^{-1}	56% after 500 cycles	This work

the capacitance calculated by the GCD using Eq. (3), was 4.13, 2.65, 1.93, 0.45, and 0.1 F at currents of 4, 6, 8, 10, and 15 mA, respectively. The specific capacitance (C_s) of the flexible EDLC based on the mass of each AC electrode calculated by Eq. (4) was 0.2 F g^{-1}.

The specific energy and power can be calculated from the GCD curve by Eqs. (5) and (6):

$$E = \frac{1}{2} C_s v^2 \quad (5)$$

$$P = \frac{E}{\Delta t} \quad (6)$$

Where E is the specific energy density, C_s is the specific capacitance, v is the potential window; P is the specific power density, and Δt is the discharging time.

The specific energy density of the EDLC printed was 0.064 Wh kg^{-1}, and specific power was 57.60 W kg^{-1}. AC based EDLCs have the unique advantage of higher power and energy density when used with organic electrolytes [31]. The specific energy of the flexible EDLC in PVA/H_3PO_4 gel electrolytes developed in this study was not comparable with organic electrolyte based EDLCs. Table 2 shows a comparison of the supercapacitor based on a 3D paste process and the supercapacitors made using other 3D printing methods. Each type of the 3D printing method has its specific advantages and disadvantages [6,32–37].

4.4. Test of combination circuits of printed flexible EDLCs

The applications of flexible EDLCs strongly depend on operating voltage. However, the maximum voltage that can be applied on a single aqueous electrolyte based EDLC is low (< 0.8 V), therefore, they often need to be connected to each other in series or parallel combinations to achieve desired operating voltage and capacitance as shown in Fig. 7(a, b). In order to demonstrate the electrical functionality of the flexible EDLCs manufactured in this study, the tests of electrical performance of two EDLCs in the form of series and parallel connection were carried out. Fig. 7(c) shows the CV curves of two individual flexible EDLCs (*C1* and *C2*) and their series and parallel combination circuits. It can be seen from curves at scan rate 20 mV s^{-1} that there is a very little reduction and oxidation at around 0.5 V in *C1*, *C2* and parallel circuits. The area of the CV curve decreased significantly for series circuits at the operating voltage of 1.6 V. It is noticed that the area of *C1* or *C2* is approximately equal to double of the area for the series circuits whereas the total area of *C1* and *C2* is equal to the area in the parallel circuit, which implies that the ELDCs behave as a normal energy storage device. Table 3 gives the relationship between the capacitance values at the scan rate of 20 mV s^{-1} and iR_{comp}. It can be seen that the flexible EDLCs made in this study behave strictly like the normal energy storage, i.e. the theoretical values are very close to the experimental values. In addition, the relationship between the capacitance values of individual EDLCs and their series and parallel circuits measured by CV and GCD tests strictly comply with the principle of energy storage. The fact that the capacitance value for series circuit (0.7/0.034 F) being lower than that for parallel circuit (2.6/0.17 F) as is expected.

The GCD plots in Fig. 7(d) shows a comparison of the first cycle charge-discharge curve for each type of circuit, i.e. two individual EDLCs and their series and parallel connection. The capacitances for *C1* and *C2* calculated from the GCD curve using Eq. (3) are 0.1 and 0.07 F, respectively. The capacitance calculated from the GCD tests for parallel circuit is 0.17 F, which is the same as the sum of *C1* and *C2* calculated by GCD. It can be seen obviously that the iR drop significantly decreases in parallel circuit, which was 0.08 V at 15 mA, in comparison with 0.36 V at the operating voltage of 1.6 V in the series circuit. The iR drop observed is larger with the series circuit due to the high value of ESR. The maximum current that can be applied in the parallel circuit at 0.8 V was identified to be 19 mA, i.e. under 19 mA and 0.8 V the parallel circuit behaves appropriately, and the iR drop increased to 0.11 V accordingly. The specific energy density of flexible EDLCs in PVA/H_3PO_4 gel electrolyte in parallel and series circuits was 0.11 Wh kg^{-1}, 0.087 Wh kg^{-1}, with power densities of 55 W kg^{-1}, 110 W kg^{-1}, respectively.

Fig. 7(e) shows that the results correspond well with the impedance performances of *C1*, *C2* and their electrical combinations in series and parallel at the frequency range of 100 kHz to 0.01 Hz. It shows a good capacitive performance even at a high frequency, e.g. 100 kHz. The semicircle cannot be seen from the graph because of the low contact resistance and highly accessible surface of the printed AC electrode; and the charge transfer resistance was low due to the electrolyte concentration. The ESR can be estimated for each circuit from the intersection between the straight section of the Nyquist plot at low frequency and the X-axis [38]. In addition, the iR_{comp} can be estimated by the same approach, but can be measured more accurately when using the auto range function in an electrochemical workstation.

4.5. Flexibility of the EDLCs

An important requirement for an energy storage device nowadays is its flexibility as conventional supercapacitors can be too bulky, heavy, and rigid. Highly flexible EDLCs that can be bent without affecting the performance are desired. Mechanical bending tests were carried out in this study to investigate the flexibility of the EDLCs printed. *C2* was chosen for the bending tests with radius (r) of 15 and 35 mm. The CV curves in Fig. 8(a) show no obvious oxidation or reduction when the current was 15 mA and the operating voltage of 0.8 V at the scan rate 50 mV s^{-1} under the conditions of being flat and with a bend radius of 35 and 15 mm. The capacitance of *C2* under those conditions was 0.68, 0.37, and 0.4 F, respectively, i.e. 54–58% of capacitance was retained under the bending conditions when compared with the original flat status. It is believed that this deterioration of capacitance was due to the adhesion between the AC electrodes and the current collector of the EDLC becoming worse under the bending condition, which caused higher resistance of the EDLC. This result is in good agreement with the findings from the results described by other researchers [39].

The GCD behaviour was also investigated at the bending radius of

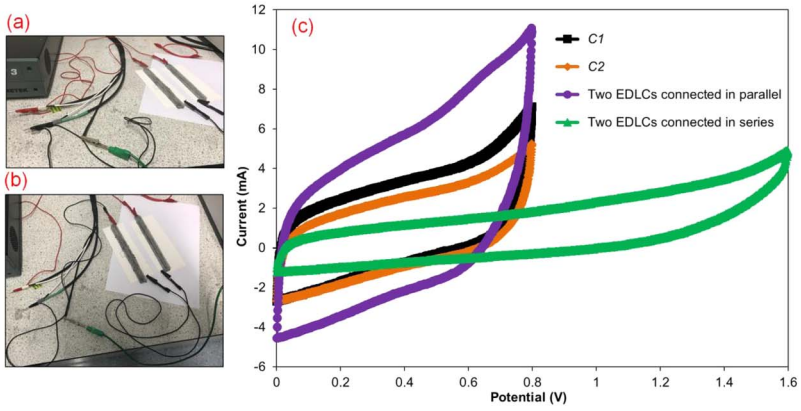

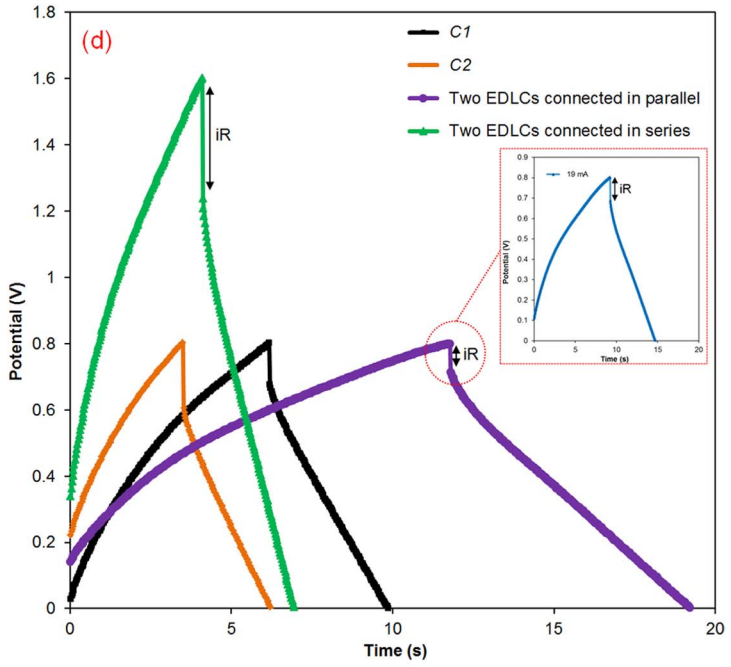

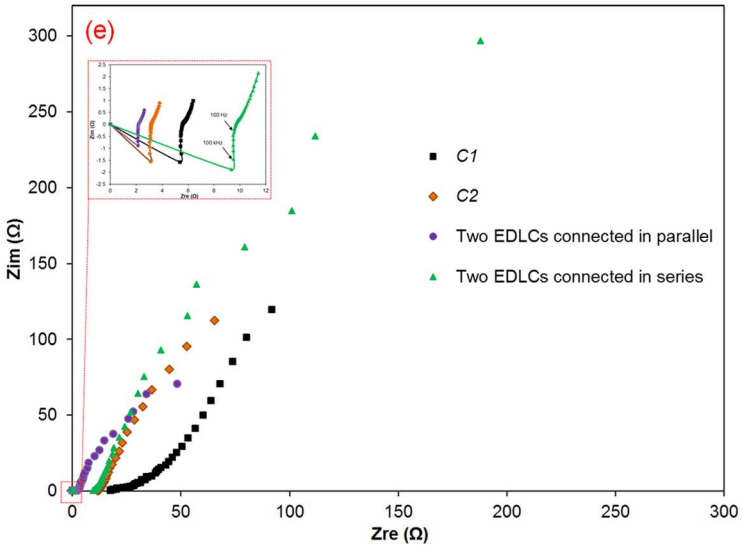

Fig. 7. (a) Photograph of two EDLCs in parallel; (b) in series; (c) CV recorded at 20 mV s^{-1} for two single EDLCs and their electrical combinations in series and parallel; (d) GCD curve of the first cycle for each circuit and enlarged view of parallel circuit at 19 mA; (e) Complex plane plot of the impedance for each circuit using a 0 V and the enlarged view in the area of high frequencies.

35 mm and 15 mm at 0.8 V and current of 15 mA, as shown in Fig. 8(b). It can be clearly seen that the iR drop significantly increases in the bent condition in comparison with the flat EDLC. The iR_{comp} also increases to 17.3 Ω at 35 mm bending radius in contrast with 13.5 Ω when the bending radius was 15 mm and 3 Ω when it was flat. Hence, the result shows that the iR_{comp} at the bending radius of 15 mm is approximately 21% less than the iR_{comp} for a radius of 35 mm, which is the reason for the slight increase of the capacitance as revealed by the CV

Table 3
All circuits calculated capacitances from CV at 20 mV s^{-1} and GCD with iR compensation.

	Capacitance (F)				iR_{comp} (Ω)
	by (CV)		by (GCD)		
	Experiment	Theory	Experiment	Theory	
C1	1.4		0.1		5.5
C2	1.5		0.07		3
Parallel	2.6	2.9	0.17	0.17	1.96
Series	0.7	0.72	0.034	0.04	8.69

measurement discussed above. The reason for iR drop change under the bending tests could be the conductivity decrease caused by the contact area change of each layer. At high bending, the iR drop decreases because of compression of the EDLC components particles.

4.6. Cycling stability and reproducibility of the EDLC by 3D printing

Fig. 9(a) shows the CV curves of *C2* for different cycles recorded at a scan rate of 80 mV s^{-1}. It can be seen that the capacitance decreases gradually when the cycling number increases. After few cycles, the contact force between electrode and PVA/H_3PO_4 gel electrolyte was changed and this suggests that the ion diffusion in the PVA/H_3PO_4 decreased as the water had evaporated. The capacitance of *C2* was calculated by Eq. (1). Fig. 9(b) shows the corresponding capacitance with respect to the CV cycle number. Capacitance decreased significantly to 80% of that initial capacitance at the 50th cycles, the capacitance was 56% compared to the capacitance at 5th cycle after 500 cycles.

The other two EDLCs (*C3* and *C4*) fabricated with the same manufacturing processes and conditions as *C1* and *C2* were evaluated by the same method to investigate the reproducibility of the 3D printing method. The performance of all four EDLCs has been compared and is shown in Fig. 9(c). It shows the typical shape of CV curves at the scan rate of 100 mV s^{-1}. The area of the CV charge and discharge curves is quite similar suggesting the stability and reproducibility of the 3D printed process for flexible EDLCs. The capacitances of all samples made are very similar at the scan rate of 20 mV s^{-1}, i.e. *C1* 1.4 F, *C2* 1.5 F, *C3* 1.4 F, and *C4* 1.2 F, respectively.

5. Conclusions

A flexible and stable electrical double layer capacitor has been developed in this study, which can be manufactured in one continuous process by a 3D printer, i.e. an extrusion system. The various materials that are needed to compose an EDLC can be applied in one extrusion system. Four EDLC samples were fabricated successfully with grid patterns by 3D printing onto flexible silicone substrate. A typical

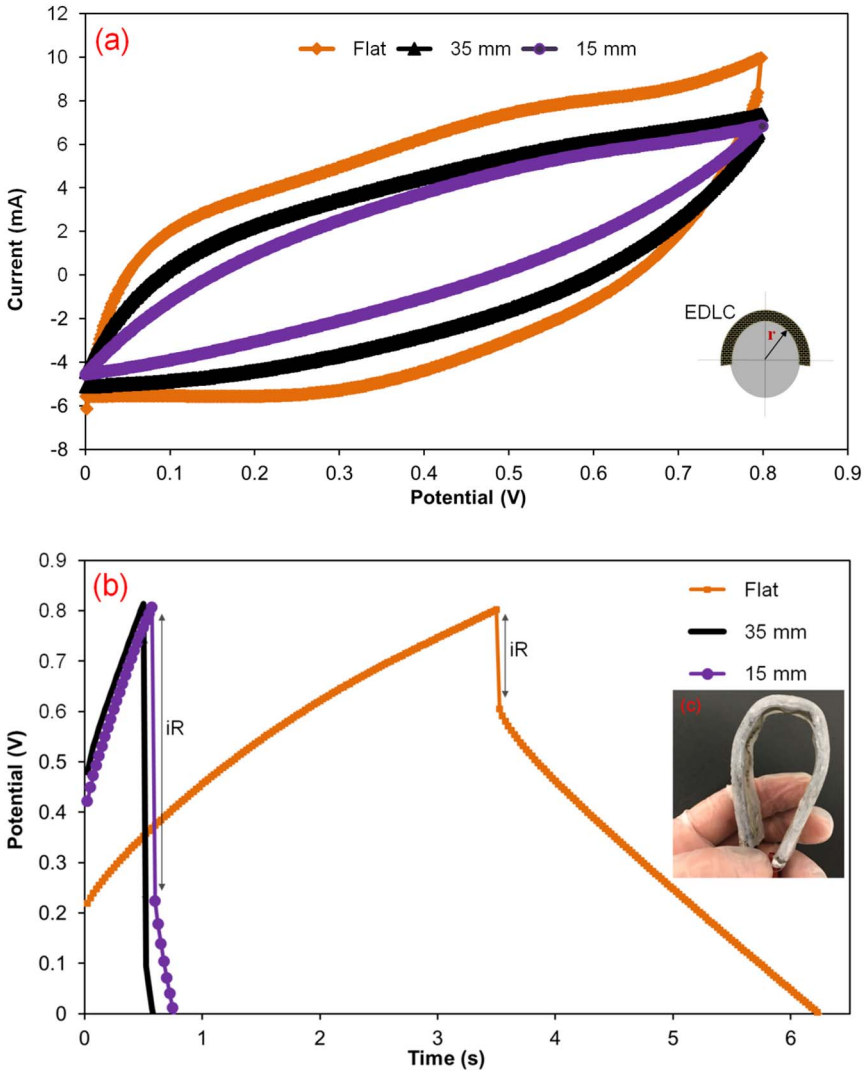

Fig. 8. (a) CV curve of 3D flexible EDLC recoded at 50 mV s^{-1} under flat, bent radius of 35 and 15 mm conditions; (b) GCD curves of flexible EDLCs with bending and flat status at current of 15 mA; (c) Digital image of flexible EDLC.

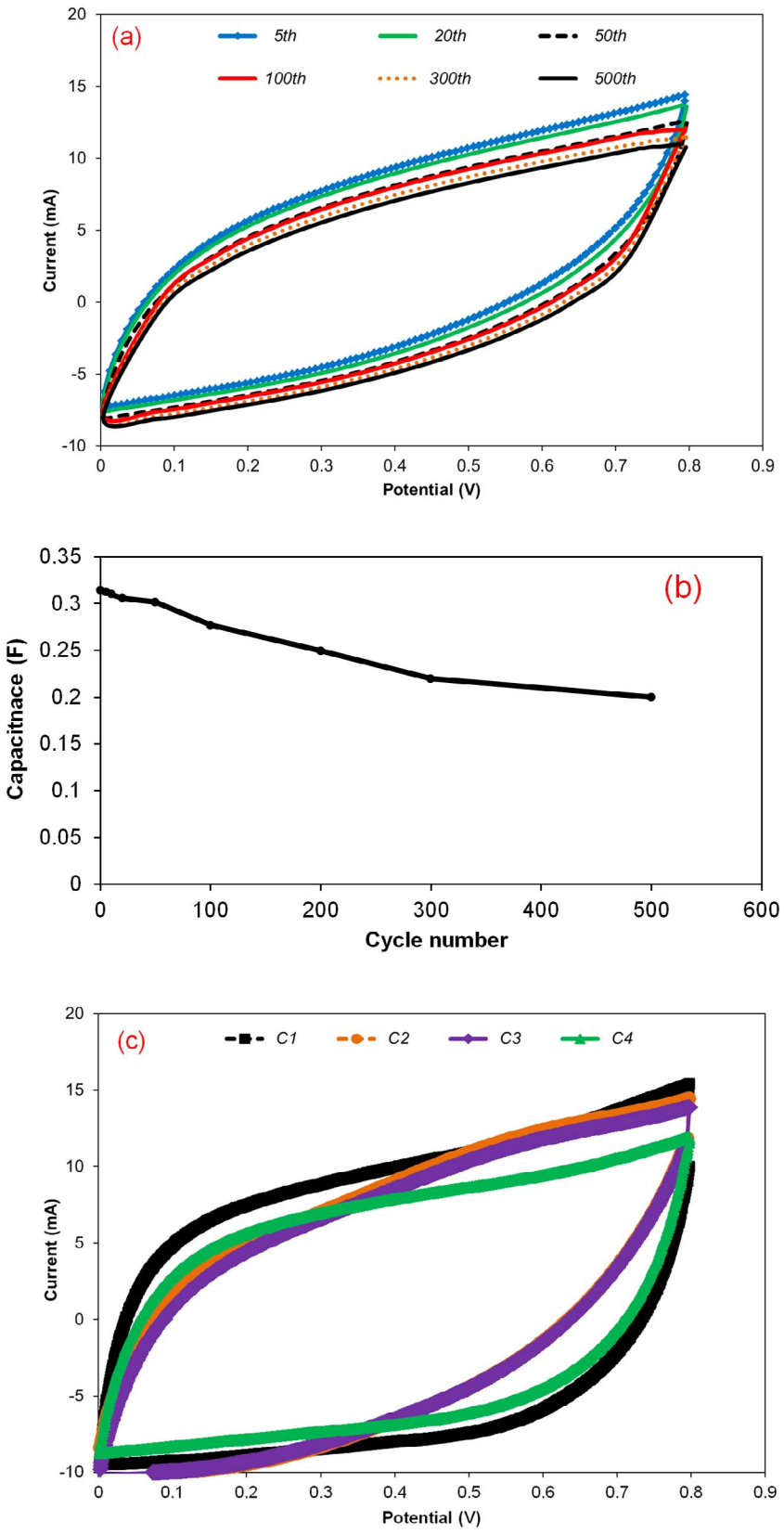

Fig. 9. (a) CV curves of the EDLC under cyclic test; (b) Capacitance decay curve of the EDLC during 500 cycles; (c) CV curves of four EDLCs under the same 3D parameters and conditions.

structure of an EDLC was created by depositing current collectors, AC electrodes, and PVA/H_3PO_4 gel electrolyte onto silicone rubber as promising flexible materials for various applications of energy storage devices. The 3D printed EDLCs exhibited an excellent electrical capacitance performance for different combination circuits. The mechanical bending of the 3D EDLC was tested and exhibited a good flexibility and retention of 54–58% of its initial capacitance at a scan rate of 50 mV s^{-1}. The 3D printing process had a good reproducibility and this suggests that 3D printing based on paste extrusion may be used to develop more sophisticated electronic devices with various forms of paste

materials.

Acknowledgement

The authors would like to thank the Ministry of Higher Education and Scientific Research of Libya for providing funds to carry out this work.

References

[1] Y. Yang, Q. Huang, L. Niu, D. Wang, C. Yan, Y. She, Z. Zheng, Waterproof, ultrahigh areal-capacitance, wearable supercapacitor fabrics, Adv. Mater. 29 (2017) 1606679, http://dx.doi.org/10.1002/adma.201606679.
[2] A. González, E. Goikolea, J.A. Barrena, R. Mysyk, Review on supercapacitors: technologies and materials, Renew. Sustain. Energy Rev. 58 (2016) 1189–1206, http://dx.doi.org/10.1016/j.rser.2015.12.249.
[3] X. Wang, X. Lu, B. Liu, D. Chen, Y. Tong, G. Shen, Flexible energy-storage devices: design consideration and recent progress, Adv. Mater. 26 (2014) 4763–4782, http://dx.doi.org/10.1002/adma.201400910.
[4] A.A. Yadav, S.N. Jadhav, D.M. Chougule, P.D. Patil, U.J. Chavan, Y.D. Kolekar, Spray deposited Hausmannite Mn3O4 thin films using aqueous/organic solvent mixture for supercapacitor applications, Electrochim. Acta 206 (2016) 134–142, http://dx.doi.org/10.1016/j.electacta.2016.04.096.
[5] M. Areir, Y. Xu, R. Zhang, D. Harrison, J. Fyson, E. Pei, A study of 3D printed active carbon electrode for the manufacture of electric double-layer capacitors, J. Manuf. Process. 25 (2017) 351–356, http://dx.doi.org/10.1016/j.jmapro.2016.12.020.
[6] G. Sun, J. An, C.K. Chua, H. Pang, J. Zhang, P. Chen, Layer-by-layer printing of laminated graphene-based interdigitated microelectrodes for flexible planar micro-supercapacitors, Electrochem. Commun. 51 (2015) 33–36, http://dx.doi.org/10.1016/j.elecom.2014.11.023.
[7] C. Meng, C. Liu, L. Chen, C. Hu, S. Fan, Highly flexible and all-solid-state paperlike polymer supercapacitors, Nano Lett. 10 (2010) 4025–4031, http://dx.doi.org/10.1021/nl1019672.
[8] F. Qiu, D. Harrison, J. Fyson, D. Southee, Fabrication and characterisation of flexible coaxial thin thread supercapacitors, Smart Sci. 2 (2014) 107–115, http://dx.doi.org/10.1080/23080477.2014.11665613.
[9] J. Smithyman, R. Liang, Flexible supercapacitor yarns with coaxial carbon nanotube network electrodes, Mater. Sci. Eng. B 184 (2014) 34–43, http://dx.doi.org/10.1016/j.mseb.2014.01.013.
[10] H. Sun, S. Xie, Y. Li, Y. Jiang, X. Sun, B. Wang, H. Peng, Large-area supercapacitor textiles with novel hierarchical conducting structures, Adv. Mater. (2016) 8431–8438, http://dx.doi.org/10.1002/adma.201602987.
[11] H.T. Jeong, B.C. Kim, M.J. Higgins, G.G. Wallace, Highly stretchable reduced graphene oxide (rGO)/single-walled carbon nanotubes (SWNTs) electrodes for energy storage devices, Electrochim. Acta 163 (2015) 149–160, http://dx.doi.org/10.1016/j.electacta.2015.02.022.
[12] J. Yeo, G. Kim, S. Hong, M.S. Kim, D. Kim, J. Lee, H.B. Lee, J. Kwon, Y.D. Suh, H.W. Kang, H.J. Sung, J.H. Choi, W.H. Hong, J.M. Ko, S.H. Lee, S.H. Choa, S.H. Ko, Flexible supercapacitor fabrication by room temperature rapid laser processing of roll-to-roll printed metal nanoparticle ink for wearable electronics application, J. Power Sources 246 (2014) 562–568, http://dx.doi.org/10.1016/j.jpowsour.2013.08.012.
[13] J. Zhang, L. Dong, C. Xu, J. Hao, F. Kang, J. Li, Comprehensive approaches to three-dimensional flexible supercapacitor electrodes based on MnO2/carbon nanotube/activated carbon fiber felt, J. Mater. Sci. 52 (2017) 5788–5798, http://dx.doi.org/10.1007/s10853-017-0813-3.
[14] A. Jain, S.K. Tripathi, Fabrication and characterization of energy storing supercapacitor devices using coconut shell based activated charcoal electrode, Mater. Sci. Eng. B 183 (2014) 54–60, http://dx.doi.org/10.1016/j.mseb.2013.12.004.
[15] J. Shieh, S. Tsai, B. Li, H. Her, High-performance flexible supercapacitor based on porous array electrodes, Mater. Chem. Phys. 195 (2017) 114–122, http://dx.doi.org/10.1016/j.matchemphys.2017.04.034.
[16] J. Shieh, C. Wu, S. Tsai, H. Her, Fabrication and characterization of a sandpaper-based flexible energy storage, Appl. Surf. Sci. 364 (2016) 21–28, http://dx.doi.org/10.1016/j.apsusc.2015.11.152.
[17] J. Shieh, S. Zhang, C. Wu, H. Her, A facile method to prepare a high performance solid-state flexible paper-based supercapacitor, Appl. Surf. Sci. 313 (2014) 704–710, http://dx.doi.org/10.1016/j.apsusc.2014.06.059.
[18] K. Choi, J. Yoo, C.K. Lee, S. Lee, All-inkjet-printed, solid-state flexible supercapacitors on paper, Energy Environ. Sci. 9 (9) (2016) 2812–2821.
[19] M.F. El-Kady, R.B. Kaner, Scalable fabrication of high-power graphene micro-supercapacitors for flexible and on-chip energy storage, Nat. Commun. 4 (2013) 1475, http://dx.doi.org/10.1038/ncomms2446.
[20] Q. Zhou, X. Ye, Z. Wan, C. Jia, A three-dimensional flexible supercapacitor with enhanced performance based on lightweight, conductive graphene-cotton fabric electrode, J. Power Sources 296 (2015) 186–196, http://dx.doi.org/10.1016/j.jpowsour.2015.07.012.
[21] S. Xu, G. Wei, J. Li, Y. Ji, N. Klyui, V. Izotov, W. Han, Binder-free Ti3C2Tx MXene electrode film for supercapacitor produced by electrophoretic deposition method, Chem. Eng. J. 317 (2017) 1026–1036, http://dx.doi.org/10.1016/j.cej.2017.02.144.
[22] S.K. Ujjain, P. Ahuja, R. Bhatia, P. Attri, Printable multi-walled carbon nanotubes thin film for high performance all solid state flexible supercapacitors, Mater. Res. Bull. 83 (2016) 167–171, http://dx.doi.org/10.1016/j.materresbull.2016.06.006.
[23] W. Zhao, M. Zhang, P. Pan, D. Song, S. Huang, J. Wei, X. Li, W. Qi, K. Zhang, J. Zhao, Z. Yang, Design and fabrication of flexible supercapacitor devices by using mesoporous carbon/polyaniline ink, Surf. Coat. Technol. 320 (2017) 595–600, http://dx.doi.org/10.1016/j.surfcoat.2016.10.075.
[24] Z. Liu, Z.S. Wu, S. Yang, R. Dong, X. Feng, K. Müllen, Ultra flexible in-plane micro-supercapacitors by direct printing of solution-processable electrochemically exfoliated graphene, Adv. Mater. 28 (2016) 2217–2222, http://dx.doi.org/10.1002/adma.201505304.
[25] Z. Zhang, J. Deng, X. Li, Z. Yang, S. He, X. Chen, G. Guan, J. Ren, H. Peng, Superelastic supercapacitors with high performances during stretching, Adv. Mater. 27 (2015) 356–362, http://dx.doi.org/10.1002/adma.201404573.
[26] W. Gao, Y. Zhang, D. Ramanujan, K. Ramani, Y. Chen, C.B. Williams, C.C.L. Wang, Y.C. Shin, S. Zhang, P.D. Zavattieri, W. Gao, The status, challenges, and future of additive manufacturing in engineering, Comput. Aided Des. 69 (2015) 65–89, http://dx.doi.org/10.1016/j.cad.2015.04.001.
[27] F.C. Godoi, S. Prakash, B.R. Bhandari, 3D printing technologies applied for food design: status and prospects, J. Food Eng. 179 (2016) 44–54, http://dx.doi.org/10.1016/j.jfoodeng.2016.01.025.
[28] H.H. Nadiyapara, Sarang Pande, A review of variable slicing in fused deposition modeling, J. Inst. Eng. (India): Ser. C 98 (2017) 387–393, http://dx.doi.org/10.1007/s40032-016-0272-7.
[29] K. Fu, Y. Yao, J. Dai, L. Hu, Progress in 3D printing of carbon materials for energy-related applications, Adv. Mater. 29 (2017) 1603486, http://dx.doi.org/10.1002/adma.201603486.
[30] M. Wei, F. Zhang, W. Wang, P. Alexandridis, C. Zhou, G. Wu, 3D direct writing fabrication of electrodes for electrochemical storage devices, J. Power Sources 354 (2017) 134–147, http://dx.doi.org/10.1016/j.jpowsour.2017.04.042.
[31] Y. Chen, X. Zhang, H. Zhang, X. Sun, D. Zhang, Y. Ma, High-performance supercapacitors based on a graphene–activated carbon composite prepared by chemical activation, RSC Adv. 2 (2012) 7747, http://dx.doi.org/10.1039/c2ra20667f.
[32] C. Zhu, T. Liu, F. Qian, T.Y.J. Han, E.B. Duoss, J.D. Kuntz, C.M. Spadaccini, M.A. Worsley, Y. Li, Supercapacitors based on three-dimensional hierarchical graphene aerogels with periodic macropores, Nano Lett. 16 (2016) 3448–3456, http://dx.doi.org/10.1021/acs.nanolett.5b04965.
[33] R. Li, R. Peng, K. Kihm, S. Bai, D. Bridges, U. Tumuluri, Z. Wu, T. Zhang, G. Compagnini, Z. Feng, A. Hu, High-rate in-plane micro-supercapacitors scribed onto photo paper using in situ femtolaser-reduced graphene oxide/Au nanoparticle microelectrodes, Energy Environ. Sci. 9 (2016) 1458–1467, http://dx.doi.org/10.1039/C5EE03637B.
[34] S. Wang, Y. Yu, R. Li, G. Feng, Z. Wu, G. Compagnini, A. Gulino, Z. Feng, A. Hu, High-performance stacked in-plane supercapacitors and supercapacitor array fabricated by femtosecond laser 3D direct writing on polyimide sheets, Electrochim. Acta 241 (2017) 153–161, http://dx.doi.org/10.1016/j.electacta.2017.04.138.
[35] C. Zhao, C. Wang, R. Gorkin, S. Beirne, K. Shu, G.G. Wallace, Three dimensional (3D) printed electrodes for interdigitated supercapacitors, Electrochem. Commun. 41 (2014) 20–23, http://dx.doi.org/10.1016/j.elecom.2014.01.013.
[36] C.W. Foster, M.P. Down, Y. Zhang, X. Ji, S.J. Rowley-Neale, G.C. Smith, P.J. Kelly, C.E. Banks, 3D printed graphene based energy storage devices, Sci Rep. 7 (2017) 42233, http://dx.doi.org/10.1038/srep42233.
[37] W. Sun, X. Chen, Fabrication and tests of a novel three dimensional micro supercapacitor, Microelectron. Eng. 86 (2009) 1307–1310, http://dx.doi.org/10.1016/j.mee.2008.12.010.
[38] C. Lei, F. Markoulidis, Z. Ashitaka, C. Lekakou, Reduction of porous carbon/Al contact resistance for an electric double-layer capacitor (EDLC), Electrochim. Acta 92 (2013) 183–187, http://dx.doi.org/10.1016/j.electacta.2012.12.092.
[39] R. Zhang, Y. Xu, D. Harrison, J. Fyson, D. Southee, A study of the electrochemical performance of strip supercapacitors under bending conditions, Int. J. Electrochem. Sci. 11 (2016) 7922–7933, http://dx.doi.org/10.20964/2016.09.59.